

# MyoScreen, a High-Throughput Phenotypic Screening Platform Enabling Muscle Drug Discovery

Joanne Young<sup>1</sup>, Yoran Margaron<sup>1</sup>, Mathieu Fernandes<sup>1</sup>,  
Eve Duchemin-Pelletier<sup>1</sup>, Joris Michaud<sup>1</sup>, Mélanie Flaender<sup>1</sup>,  
Oana Lorintiu<sup>1</sup>, Sébastien Degot<sup>1</sup>, and Pauline Poydenot<sup>1</sup>

## Abstract

Despite the need for more effective drug treatments to address muscle atrophy and disease, physiologically accurate in vitro screening models and higher information content preclinical assays that aid in the discovery and development of novel therapies are lacking. To this end, MyoScreen was developed: a robust and versatile high-throughput high-content screening (HT/HCS) platform that integrates a physiologically and pharmacologically relevant micropatterned human primary skeletal muscle model with a panel of pertinent phenotypic and functional assays. MyoScreen myotubes form aligned, striated myofibers, and they show nerve-independent accumulation of acetylcholine receptors (AChRs), excitation–contraction coupling (ECC) properties characteristic of adult skeletal muscle and contraction in response to chemical stimulation. Reproducibility and sensitivity of the fully automated MyoScreen platform are highlighted in assays that quantitatively measure myogenesis, hypertrophy and atrophy, AChR clusterization, and intracellular calcium release dynamics, as well as integrating contractility data. A primary screen of 2560 compounds to identify stimulators of myofiber regeneration and repair, followed by further biological characterization of two hits, validates MyoScreen for the discovery and testing of novel therapeutics. MyoScreen is an improvement of current in vitro muscle models, enabling a more predictive screening strategy for preclinical selection of the most efficacious new chemical entities earlier in the discovery pipeline process.

## Keywords

in vitro skeletal muscle model, high-content screening, drug discovery, muscle regeneration, excitation–contraction coupling

## Introduction

During human skeletal muscle generation and repair, nascent myotubes mature into myofibers, with internal reorganization of myofilaments into sarcomeres to form myofibrils, establishment of monosynaptic innervation, and structural maturation of the excitation–contraction coupling (ECC) apparatus.<sup>1–3</sup> During aging and certain diseases, a decline of muscle mass and strength occurs characterized by myofibrillar protein degradation, denervation, atrophy, and deterioration in neuromuscular function.<sup>4–6</sup> The development of therapeutic agents and nutritional supplements that block or attenuate muscle wasting would benefit a diverse set of clinical conditions and improve patient quality of life.

In vitro, myogenesis can be triggered in confluent two-dimensional (2D) myoblast cultures by withdrawal of growth factors from the growth medium. Unlike parallel myofibers of intact muscle, however, the resulting myotubes are randomly oriented and often branched, and they

recapitulate only the early stages of myogenesis. One principal cause is uniform tissue-culture surfaces that cannot provide stable microenvironmental cues for proper cell alignment during differentiation, an arrangement that is vital for muscle functionality, affecting myofibrillogenesis to contraction.<sup>7–9</sup> The lack of native muscle architecture and physiology limits the predictive value of these models for muscle drug discovery, and it is one reason why apparently promising drug candidates later fail to translate into clinical success.

---

<sup>1</sup>CYTOO SA, Grenoble, France

Received Nov 13, 2017, and in revised form Jan 18, 2018. Accepted for publication Jan 30, 2018.

Supplementary material is available online with this article.

### Corresponding Author:

Joanne Young, CYTOO SA, Minatéc – BHT – Bât 52, 7 parvis Louis Néel, 38030 Grenoble cedex 9, France.  
Email: jyoung@cytoo.com

Generation of mature myotubes for screening in 96- and 384-well plates presents additional challenges. Myotube differentiation is typically heterogeneous due to patchy formation of confluent cultures resulting from uneven seeding. The most significant barrier, however, especially for implementation of high-content screening (HCS) using imaging of cultured myotubes, is achieving sufficient robustness necessary for mapping phenotypic responses to pharmacological perturbations. Frequently, the extreme population morphological heterogeneity and overlapping of structures in the monolayer prevent accurate automated image segmentation and extraction of morphological parameters from individual cells.<sup>10,11</sup>

Combining a 2D culture of myoblasts with topographical constraints, elastic surfaces, neuronal coculture, mechanical stretch, electrical stimulation, or use of 3D engineered muscle bundles has progressed myotube functionality *in vitro*.<sup>12</sup> Along with improvements in cell-culture media formulation, some laboratories have even managed to grow myotubes that reach maturation levels equivalent to perinatal-stage muscle.<sup>13–17</sup> These advanced models have had little impact on drug-screening campaigns, however, due to drawbacks in scalability, workflow integration, and number of primary cells required for assembly.<sup>18–20</sup> As a result, muscle drug discovery approaches have remained limited to target-based screening in nonmuscle cells<sup>21</sup> or rodent myoblasts,<sup>22–24</sup> or, rarely, single phenotypic endpoint screening in myotubes.<sup>10</sup> A noteworthy exception is the significant contribution to preclinical drug screening by Vandenberg and colleagues, who constructed miniature 3D dystrophic muscles in prototype 96-well plates, allowing the effects of 31 compounds at six concentrations to be measured on contractile force generation.<sup>25</sup> Nevertheless, single endpoint measurements provide minimal information, miss potential beneficial or adverse effects of a compound, and cannot be exploited for predicting the mechanism of action (MOA). Thus, a biomimetic musculoskeletal model requiring few primary cells that is amenable to automated high-throughput (HT) drug screening and imaging with quantification of complex phenotypes in both primary and secondary screening modes is a current unmet need.

Strategically, the ideal *in vitro* muscle drug discovery platform should use striated, contractile human myofibers; offer comparative screening on well-characterized donors; and combine a suite of robust assays that quantitatively analyze drug effects on relevant metrics such as myoblast proliferation, myogenesis, maturation, viability, hypertrophy and atrophy, acetylcholine receptor (AChR) functionality, ECC, and contraction. The present study reports such a breakthrough with the creation of MyoScreen, the first robust and versatile muscle drug discovery platform that incorporates a mature myotube model with functional assays exhibiting exceptional performance characteristics.

## Materials and Methods

### Reagents

Primary antibody dilution and sources are referenced in **Supplementary Table S1A**. Corresponding Alexa Fluor488- or 647-conjugate polyclonal secondary antibodies were used per supplier's instructions (Jackson ImmunoResearch, Suffolk, UK). Hoechst 33342 (H3570, Invitrogen, Courtaboeuf, France) was used to stain nuclei. Positive control reagents included dexamethasone (D4902), tumor necrosis factor- $\alpha$  (TNF $\alpha$ ; T6674), and cerivastatin (SML0005) from Sigma-Aldrich (St-Quentin-Fallavier, France); interleukin-1 $\beta$  (IL1 $\beta$ ; 200-01B) and myostatin (120-00) from Peprotech (Neuilly-sur-Seine, France); trichostatin A (TSA; BML-GR309), insulin-like growth factor-1 (IGF1; ADI-908-059-0100), simvastatin (BML-G244-0050), fluvastatin (ALX-270-466-M010), and lovastatin (BML-G226-0010) from Enzo Life Sciences (Villeurbanne, France); transforming growth factor- $\beta$ 1 (TGF $\beta$ 1; 240-B-002/CF) from R&D Systems (Lille, France); and atorvastatin (3776) and pravastatin (2318) from Tocris (Lille, France). The Prestwick Chemical Library consists of 1280 US Food and Drug Administration (FDA)-approved and -marketed drugs (651201-PW, Prestwick Chemical, Illkirch, France). The Library of Pharmacologically Active Compounds (LOPAC<sup>1280</sup>) contains 1280 compounds that are mostly marketed drugs and failed development candidates (LO3300, Sigma-Aldrich). Cell viability was measured using CellTiter-Glo (G7571, Promega, Charbonnières-les-Bains, France) according to kit instructions.

### Cell Culture Maintenance

Primary human skeletal muscle myoblasts (HSMMs; CC-2580, Lonza, Basel, Switzerland, or CBC Biotec Centre de Ressources Biologiques, Hospices Civils de Lyon, Lyon, France) sourced from different donors (**Suppl. Table S2**) were cultured for six passages in growth medium (SkGM-2 BulletKit CC-3245, Lonza). Cultures were expanded and frozen stocks prepared following the vendors' instructions. Cells were maintained in a humidified incubator at 37 °C, 5% CO<sub>2</sub>, and passaged when they reached 70–80% confluence, about every 4 days.

### High-Throughput Myotube Formation

All steps were accomplished automatically using a Freedom EVO150 workstation (Tecan, Männedorf, Switzerland). For the primary drug screen and contractile activity assay, 10,000–15,000 HSMMs per well were seeded in growth medium in 96-well MyoScreen CYTOOplates (CYTOO, Grenoble, France) coated with 20  $\mu$ g/ml fibronectin (33010018, Invitrogen). Produced using CYTOO's proprietary micropatterning technology, these black-framed,

glass-bottomed microplates are standard Society for Laboratory Automation and Screening (SLAS) format. Each well contains approximately 100 micropatterns of 0.5 mm length, and a specific geometry that provides cell spatial confinement and local microenvironmental signals, resulting in standardized myotube formation and morphology. Micropatterns are separated by nonadhesive areas that prevent cell spreading to ensure long-term functional organization of myotubes. After 20 h, growth medium was changed to differentiation medium (DM) composed of Dulbecco's Modified Eagle Medium: Nutrient Mixture F12 (DMEM/F12; 31331028, Invitrogen), 0.1% horse serum (HS; B15023, GE Healthcare, Vélizy-Villacoublay, France), 50 U.mL<sup>-1</sup> penicillin, and 50 mg.mL<sup>-1</sup> streptomycin (15140122, Invitrogen). The next day, DM was refreshed, and compounds were added for 96 h. For the benchmark test, all of the above steps were performed using SensoPlates (655892, Dutscher, Brumath, France). For assays concerning AChR clusters, calcium transients, and ECC coupling, higher maturation levels were favored by differentiating in DM containing 2% HS, and experiments performed on myotubes differentiated during 8 or 9 days.

### *Immunocytochemistry and High-Resolution Microscopy*

Following 30 min fixation in 10% formalin (HT5014, Sigma-Aldrich), myotubes were washed three times in Dulbecco's Phosphate-Buffered Saline (DPBS; 14190169, Invitrogen) and permeabilized in 0.1% Triton X-100 (T9284, Sigma-Aldrich). After blocking in 1% bovine serum albumin (BSA; A7906, Sigma-Aldrich), cells were incubated with primary antibodies (**Suppl. Table S1**) for 90 min at room temperature and washed three times in DPBS. Secondary antibodies were added for 1 h with Hoechst 33342. Cells were washed three times in DPBS before acquisition. A DMI6000 (Leica Microsystems, Nanterre, France) or Eclipse-Ti (Nikon, Champigny-sur-Marne, France) wide-field microscope controlled by Metamorph software (Molecular Devices, Sunnyvale, CA, US), and equipped with digital C8484 or ORCA-R2 charge-coupled device (CCD) cameras, respectively (Hamamatsu, Bridgewater, NJ, US), was used for video-imaging and when higher spatial resolution was required. Films, color composite images, and look-up table displays were generated using ImageJ.<sup>26</sup>

### *High-Content Phenotypic Screening*

After fixation and immunostaining (**Suppl. Table S1**), quantitative microscopy was performed using the Operetta HCS imaging system with a 10×/0.3 NA objective (PerkinElmer, Courtaboeuf, France). Images were analyzed using scripts developed in Acapella software (PerkinElmer),

including customized segmentation of myotubes and nuclei. Micropatterned and conventional myotubes were defined as areas positive for skeletal muscle differentiation markers fast-myosin heavy chain (fast-MHC) or troponin T and conforming to specific filters optimized for each culture system. Filters to identify nonpatterned myotubes were based on areas that are greater than a minimum intensity threshold and contain two or more nuclei. For patterned myotubes, additional stringent properties were calculated, including the min/max area, maximum orientation, minimum elongation, and min/max length of myotubes. A nuclei count was performed to define the total number of nuclei. The fusion index (FI) was calculated as the number of nuclei within the myotube staining area divided by the total number of nuclei and expressed as a percentage. After exclusion of myotubes touching the image borders, whole entire myotubes were finally used to extract size parameters, including myotube area, myotube width, and number of nuclei per myotube.

### *AChR Clustering Assay*

Myotubes were treated with 0.5 or 5 nM rat recombinant agrin (550-AG-100, R&D Systems) for 16–20 h before fixation. Immunostaining (**Suppl. Table S1**) was as described above except that 0.1% Triton X-100 was included in all steps apart from DPBS washes. Images were acquired on the Operetta at 20×/0.45 NA objective magnification and analyzed using Acapella. Segmentation of nuclei and myotubes generated information about the cell count and FI. AChR clusters of >60 μm<sup>2</sup> were detected based on segmentation of regions with a high density of maxima points. The number and average area of AChR clusters were calculated, as well as the total area normalized per square millimeter of myotube area.

### *Calcium Flux Assay*

Cells were washed with calcium buffer containing in millimolar (mM): 130 NaCl, 5.4 KCl, 1.8 CaCl<sub>2</sub>, 0.8 MgCl<sub>2</sub>, 5.6 D-glucose, 10 HEPES, pH 7.4. Cells were then incubated for 1 h with 2 μM Fluo-4 AM (F14201, Invitrogen) in an incubator (37 °C, 5% CO<sub>2</sub>). After washing to remove unloaded dye, myotube responses to 20 μM acetylcholine (ACh; A6625, Sigma-Aldrich), 20 mM KCl, 10 mM caffeine (C0750, Sigma-Aldrich), or 400 μM 4-CmC (C55402, Sigma-Aldrich) were video-imaged. Stream acquisitions were set at 1 s intervals, and one field of view was acquired per well. Pretreatment with inhibitors tubocurarine (T2379, Sigma-Aldrich), nifedipine (N7510, Sigma-Aldrich), or ryanodine (ALX-630-062-M001, Enzo Life Sciences) was performed 15 min before ACh treatment. In experiments using calcium-free buffer, CaCl<sub>2</sub> was replaced by 2 mM EGTA and added by washing myotubes four times just before ACh addition to minimize depletion of intracellular

calcium stores. Images were processed and analyzed automatically using a dedicated software developed in-house that integrates the open-source ImageJ framework.<sup>26</sup> The image analysis tool segments myotubes in images acquired throughout time in the same well. The Fluo-4 total fluorescence intensity is measured inside each myotube and corrected for background. The total intensity is normalized to the myotube area to obtain the mean fluorescence intensity for each myotube. For data presentation, kinetic curves of calcium response are expressed as time ( $x$ -axis) versus the ratio  $F/F_0$  ( $y$ -axis), where  $F$  is the mean fluorescence intensity normalized to  $F_0$ , the baseline mean fluorescence intensity measured before compound addition.

### Contractile Activity Assay

Cells were washed with calcium buffer as above. Myotube contraction was induced by addition of 100  $\mu$ M ACh for 3 min, after which myotubes were fixed and immunostained with troponin T antibody. Optional tubocurarine pretreatment was added 15 min before contraction induction. Automated acquisition was performed on the Operetta platform with a 10 $\times$ /0.3 NA objective. Detaching myotubes were automatically detected and quantified using Acapella, based on the detection of high-intensity regions within the edges of segmented myotubes that mark the spots where the myotubes detached.

### Statistical Evaluation

Data are shown as mean  $\pm$  standard deviation (SD) and represent a minimum of two independent experiments. Prism v6 (GraphPad Software, La Jolla, CA, US) was used for statistical comparisons performed as indicated in figure legends, to fit sigmoidal dose–response curves using a variable-slope four-parameter logistic algorithm and determine  $EC_{50}$  and  $IC_{50}$ . Significance was set at  $p < 0.05$ .

## Results

### *Micropatterned Myotubes Outperform Conventionally Cultured Myotubes, Showing Enhanced Differentiation and Improved Maturation*

To emulate the functional architecture of muscle fascicles as closely as possible, a unique micropattern shape was designed that promotes the formation of parallel aligned myotubes (**Fig. 1A**). Subsequent tests using the same density of myoblasts (10,000 cells per well; female donor, age 16 years), seeded into conventional 96-well nonpatterned (NP plates) or micropatterned plates (CYTOOplates), showed that myotube formation initiated earlier on micropatterns (**Fig. 1A**). Thus, in CYTOOplates, organized elongated myotubes expressing

fast-MHC were visible by 24 h post differentiation and continued to grow during the next 48 h. Meanwhile, in NP plates, isolated short myotubes emerged later, at 48 h post differentiation. Quantitative measurement of the kinetics of myotube formation using ImageJ confirmed the higher efficiency of myogenic differentiation in CYTOOplates, with an FI that was 11-fold, 2.6-fold, and 1.7-fold more than in NP plates after 1, 2, and 3 days of differentiation, respectively (mean FI  $\pm$  SD after 3 days of differentiation:  $69 \pm 3\%$  vs.  $40 \pm 1\%$ ; **Fig. 1B**). Similarly, the median myotube width at 5 days post differentiation was larger in CYTOOplates than NP plates ( $37 \pm 11 \mu$ m vs.  $28 \pm 14 \mu$ m; **Fig. 1C**). Most strikingly, the normalizing environment of the micropatterned CYTOOplates significantly reduced intra- and interwell variability of myotube size by fivefold compared to NP plates, where uncontrolled cell fusion resulted in a heterogeneous myotube population (**Fig. 1C**).

Micropatterned myotubes also developed more extensive intracellular myofibrils compared to myotubes formed on isotropic surfaces. This was assessed by manual counting of myotubes showing a striated pattern indicative of sarcomeres after fast-MHC immunostaining of thick filaments (**Fig. 1D**). The number of sarcomeric myotubes was >sixfold higher in CYTOOplates compared to NP plates after 3 days of differentiation ( $61 \pm 18\%$  vs.  $9 \pm 7\%$ ; **Fig. 1D**). By day 5 of differentiation, other sarcomeric proteins likewise showed a striated pattern, including  $\alpha$ -actinin that labels Z-lines and troponin T associated with thin filaments (**Fig. 1E**). The localization of dystrophin continuously along the subsarcolemma also implies that micropatterned myotubes have attained an advanced degree of differentiation (**Fig. 1E**).

The above side-by-side comparison shows that in micropatterned CYTOOplates, myoblasts exhibit faster differentiation kinetics leading to more mature myotubes than in NP plates. The same number of cells per well are plated in both plates, and although CYTOOplates have a reduced area available for cell adherence, meaning myoblasts will reach confluence more rapidly on micropattern islets, cell density is not the only parameter influencing differentiation. The geometrically controlled microenvironment that provides spatial cues guiding myoblast–myotube alignment significantly contributes to increased fusion and maturation efficiency, as previously shown by others.<sup>27–29</sup> The CYTOOplate cell-culture system also bestows additional benefits over conventional cultures for screening. This includes use of fewer precious primary myoblast cells, generation of a more synchronous and homogeneously sized myotube population, reduced assay setup time because myotubes show relevant phenotypes earlier, and the possibility to extend culture timelines to achieve further maturation. Indeed, myotubes with standardized morphology persisted in CYTOOplates for at least 12 days post differentiation without detachment or loss of viability (data not shown).

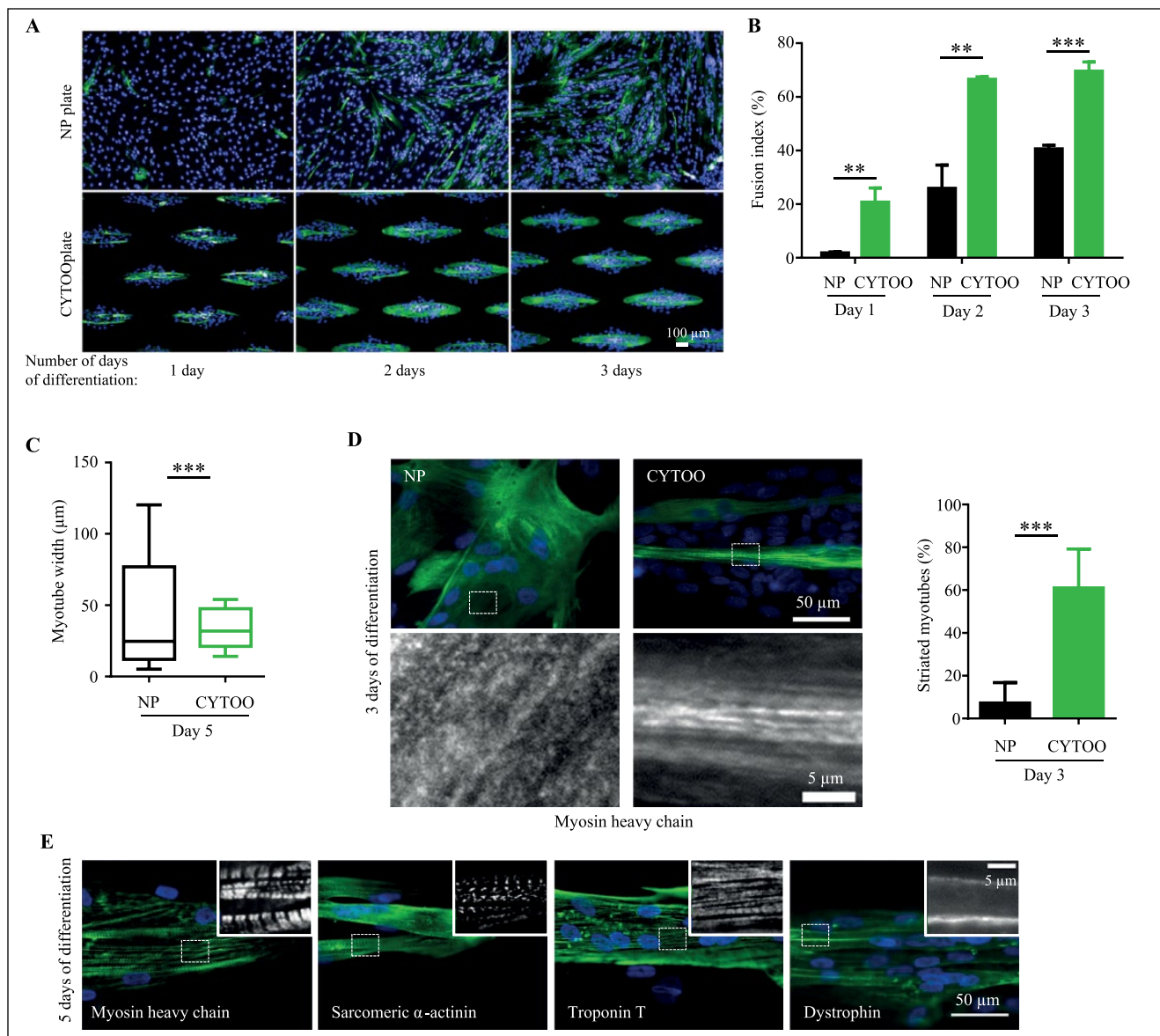


**Figure 1.** Improved myogenesis and maturation kinetics on micropatterned 96-well CYTOOplates. **(A)** Fluorescent images of myotubes formed during a 3-day time course of differentiation in nonpatterned (NP) and micropatterned (CYTOO) 96-well plates. Myotubes were immunolabeled for fast-myosin heavy chain (fast-MHC; green), and nuclei were counterstained with Hoechst (blue). Images were taken with an Operetta high-content screening (HCS) system using the 10 $\times$  objective. **(B)** Quantification of the fusion index (FI) during the first 3 days of differentiation in NP plates and CYTOOplates, as determined by the percentage of nuclei occurring within myotubes.  $n = 3$  wells;  $**p \leq 0.01$ ,  $***p \leq 0.001$  in a Student's  $t$ -test. **(C)** Measurement of myotube width after initiation of differentiation during 5 days in NP plates versus CYTOOplates. Box plot represents the median and 25th to 75th percentiles, and outer bars show the 10th to 90th percentiles. Data show the variation within individual myotubes measured from nine wells per condition.  $***p < 0.001$  by a Student's  $t$ -test. **(D)** Higher percentage of striated myotubes on CYTOOplates. Manual quantification of the number of striated myotubes based on MHC staining pattern and visual examination under the microscope. Myotubes were differentiated during 3 days on 96-well NP plates or CYTOOplates. Representative images of MHC staining (green) in myotubes from each culture system are shown on the left, with magnifications of white insets displayed below in grayscale. Note the well-aligned myofibrils in the CYTOOplate myotubes.  $n = 3$  wells;  $***p \leq 0.001$ , as analyzed by Student's  $t$ -test. **(E)** Myotube maturation characterized by the expression and distribution of contractile muscle proteins after 5 days of differentiation on micropatterns. Myotubes were stained with antibodies against fast-MHC,  $\alpha$ -actinin, and troponin T that show a striated pattern and the cytoskeletal protein dystrophin that lines the inner sarcolemma (all in green). Nuclei are counterstained with Hoechst (blue). Images were manually acquired with a Leica wide-field microscope using a 20 $\times$ /0.7 NA objective. Small white boxes indicate an area that is magnified in insets displayed on the top right of each picture. A 16-year-old female donor was used for this part of the study.

## MyoScreen HCS Pipeline Development

To streamline processes, quantitative image acquisition and analysis of changes in myotube morphology were implemented on the Operetta imaging system using custom Acapella scripts and just two imaging channels to identify nuclei and myotubes, as outlined in **Supplemental Figure S1A**. Eleven fields per well imaged with a 10 $\times$  objective ensured analysis of >5750 micropatterns/96-well plate with each pattern organizing multiple myotubes, thus providing robust statistics while maximizing throughput. Images were processed with computing on a per-micropattern basis, and data output was presented as a mean of triplicate wells. Compared to NP myotubes that are difficult to analyze individually, images of multiple horizontally aligned myotubes with standardized orientation and morphology could be segmented and analyzed without application of tedious image-processing routines, accelerating measurement of descriptors including number of myotubes, FI, mean myotube size, myonuclei per myotube, and mean fluorescence intensity of differentiation markers. When comparing drug response between conventionally grown and micropatterned myotubes, micropatterned myotubes showed a significantly higher response due to the more accurate image analysis detection of atrophy and especially hypertrophy phenotypes, increasing the dynamic range of the assay signal windows (+22% vs. +7%, respectively, after IGF1 treatment; **Suppl. Fig. S1B**). Therefore, use of micropatterned myotubes will more likely result in uncovering of novel candidates that enhance fusion efficiency or induce hypertrophy compared to use of conventionally cultured myotubes. The established myotube model and HCS platform was assigned the name MyoScreen.

The universality of the automated MyoScreen protocol (**Suppl. Fig. S2**) was evaluated using HSMs isolated from four different donors (2 female and 2 male, ages 4 to 68 years; **Suppl. Table S2**). Myoblasts from all individuals formed myotubes (**Fig. 2A**), but their capacities to proliferate (number of nuclei) and differentiate (FI) and the size of the myotubes (myotube mean area) were clearly reduced with increasing donor age (**Fig. 2B**), in agreement with similar reports.<sup>30</sup> MyoScreen can thus discern phenotypic differences between myoblasts or myotubes isolated from donors of different ages.

## MyoScreen Predicts Expected Drug Effects

To assess the pharmacological relevancy of MyoScreen, myoblasts from a healthy adult donor (male, 21 years) were characterized for sensitivity to 13 well-established inducers of muscle hypertrophy or atrophy. Compounds were added during early differentiation and incubated for 4 days without medium change, according to the workflow in **Supplemental Figure S2**. Dose responses for FI, myotube area, and nuclei count to monitor toxicity were plotted as percentage increases or decreases compared to untreated controls fixed at 100%, and EC<sub>50</sub> and IC<sub>50</sub> values were calculated from fitted curves

(**Suppl. Table S3**). All compounds tested showed the same effects as described in vivo. Hence, exposure of differentiating myotubes to the highly anabolic hormone IGF1 (PI3K–Akt–mTOR signaling pathway; **Fig. 3A** and **3E**) or the histone deacetylase inhibitor trichostatin A (TSA; **Suppl. Fig. S3A**) resulted in  $\geq$ 50% increase of the differentiation rate and size of myotubes. TSA was effective within a narrower concentration window (200–400 nM), as expected, given the large variety of biological effects caused by histone deacetylase (HDAC) inhibition. Factors causing muscle-wasting disease in vivo induced antimyogenic effects in vitro. Thus, proinflammatory cytokines TNF $\alpha$  and IL1 $\beta$  that activate nuclear factor- $\kappa$ B-mediated signaling and two TGF $\beta$  superfamily members, TGF $\beta$ 1 and myostatin, that converge onto the same pathway activating Smad2/3 all reduced cell fusion and produced smaller myotubes, while maintaining cell viability (**Fig. 3B**, **3C**, and **3E** and **Suppl. Fig. S3B** and **S3C**). Furthermore, common medications such as glucocorticoid dexamethasone and lipid-lowering simvastatin, known to produce side effects of myopathy,<sup>31</sup> also induced concentration-dependent atrophy in vitro, suggesting equivalent activities occurring in vitro and in vivo (**Fig. 3D** and **3F**). Levels of atrophy and myotoxicity induced by six different statins (0.1–100  $\mu$ M) reflected their relative lipophilicity, with highest levels for cerivastatin (withdrawn in 2001) and simvastatin and zero negative effects for pravastatin, consistent with incidences of rhabdomyolysis observed for these statins in clinical situations (**Fig. 3F**).<sup>32</sup> Overall, these results establish the predictive ability of MyoScreen to identify compounds inducing hypertrophy or atrophy through distinct signaling pathways.

To determine assay robustness, Z'-factor<sup>33</sup> was calculated for multiple plates. A typical MyoScreen assay validation plate and results are shown in **Supplemental Figure S3D** and **S3E**. Myotubes (male, 21 years) exposed to 12.5 nM IGF1, 2.3 nM TNF $\alpha$ , or medium-only controls produced values of 0.63 and 0.57, respectively, for the endpoint of FI, well within the acceptable range for HCS. In addition, coefficients of variation (CVs) were less than 15%, illustrating low variation between well replicates ( $n = 32$  wells per condition). So far, MyoScreen provides phenotypic descriptors that are reliable indicators of myotube development and maturation. The maturity of the model was further investigated with the goal of integrating additional assays related to neuromuscular junction (NMJ) formation, ECC, and contraction.

## MyoScreen Myotubes Develop Spontaneous Agrin-Responsive AChR Clusters Necessary for NMJ Formation

Contrary to in vitro animal myotubes, there are no known reports of AChR cluster detection in conventionally cultured aneural human primary myotubes. Consequently, their ability to spontaneously accumulate AChRs is thought

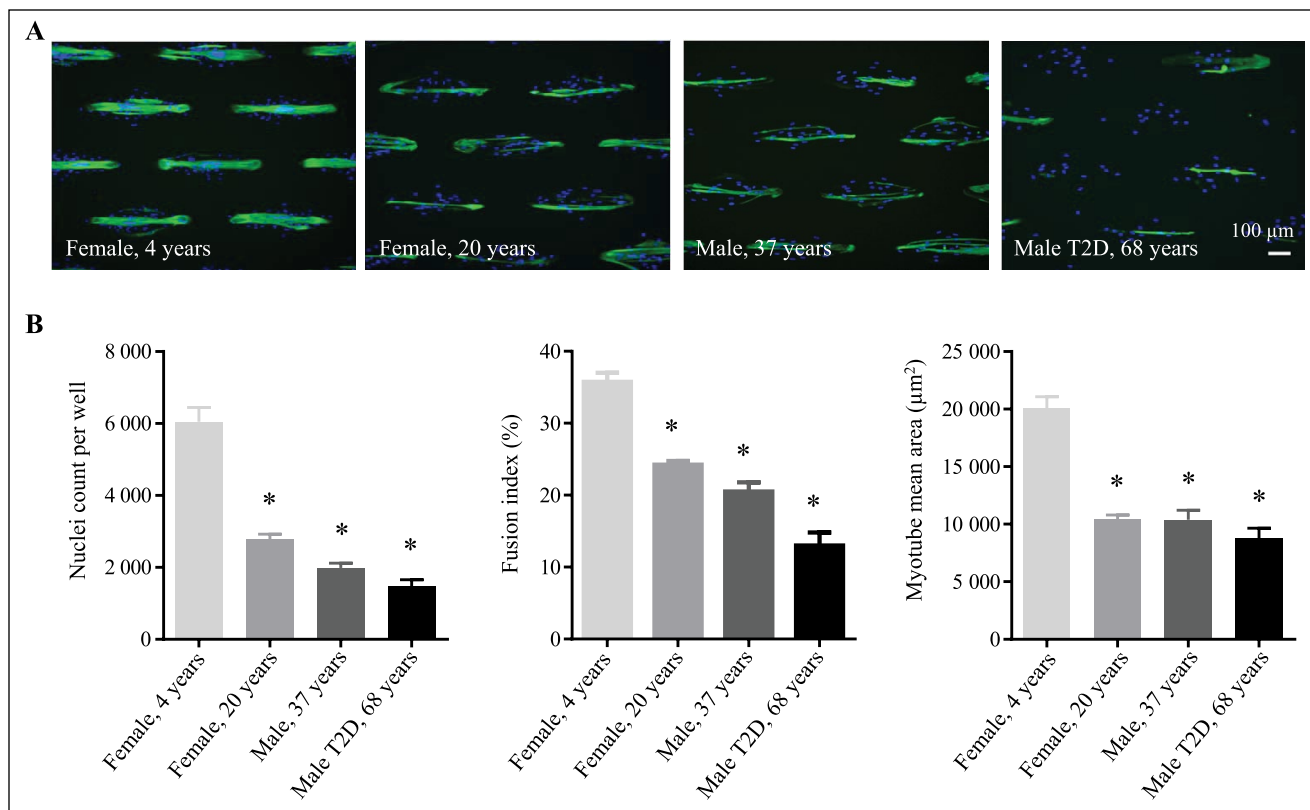


**Figure 2.** Validation of MyoScreen myotube formation and imaging protocols in myoblasts obtained from donors of different ages. **(A)** Representative automatically acquired images of cultured MyoScreen human primary myotubes from donors with a broad age range. Myotubes and nuclei are stained with troponin T antibody (green) and Hoechst (blue), respectively. **(B)** Effect of donor age on myoblast and myotube proliferation, differentiation rate, and size. Data represent mean  $\pm$  SD ( $n = 4$  wells) and were compared to the youngest donor's myotubes using the Mann–Whitney nonparametric test. \* $p < 0.05$ . In both **(A)** and **(B)**, myotubes were differentiated for 6 days in differentiation medium containing 0.1% horse serum.

to be neuron dependent.<sup>34</sup> Remarkably, when labeled with a specific anti-AChR antibody, MyoScreen myotubes (female, 4 years) at 8 days post differentiation displayed AChR clusters punctuated along the sarcolemma membrane in the middle of the myotube fiber and in distinct regions at the ends of myotubes (**Fig. 4A**). To develop an automated AChR cluster assay, an AChR detection routine was developed that was sensitive and robust enough to analyze aggregate number and size clusters in images using the Operetta–Acapella system (see Materials and Methods).

An early hallmark of postsynaptic differentiation at the NMJ *in vivo* is AChR clustering in response to agrin, a synaptogenic proteoglycan secreted by neurons.<sup>2</sup> Addition of 5 nM agrin to day 7 differentiated MyoScreen myotubes (female, 4 years) for 16 h slightly but significantly increased the number of AChR clusters by 1.2-fold from  $368 \pm 17$  to  $442 \pm 19$  clusters per mm<sup>2</sup> of myotube area (**Fig. 4B**). A more marked effect was obtained on the average cluster size, which increased 1.68-fold from  $434 \pm 27$  to  $730 \pm 60$  μm<sup>2</sup>, and on the total area of AChR clusters, which augmented twofold from  $159,436 \pm 4060$  to  $322,019 \pm 14,056$

μm<sup>2</sup>/mm<sup>2</sup> of myotube area (**Fig. 4B**). These data indicate that stabilization of preexisting AChR clusters by agrin occurs in MyoScreen myotubes, analogous to the NMJ postsynaptic apparatus *in vivo*. To test the validity for screening of an assay to quantify modulation of AChR clusters, the Z<sup>2</sup>-factor was calculated from 30 medium-only control wells and 30 agrin-treated wells from more than three separate CYTOOplates (data not shown). Using agrin as a reference against background and the most stable imaging parameter, namely AChR total cluster area, the average Z<sup>2</sup>-factor was  $>0.4$  and controls had CVs of 9–12%, indicating an assay with high sensitivity and reproducibility.

These data demonstrate for the first time that human myotubes can form AChR clusters in the absence of innervation. Likely, AChRs were not observed previously due to the poor maturation status of conventionally grown human myotubes, providing further evidence for the improved biomimicry of MyoScreen myotubes. Morphologically, AChR-rich clusters in control and agrin-treated myotubes resemble plaque-stage aggregates (**Fig. 4A**) that are the precursors of more mature pretzel-like structures observed occasionally under these

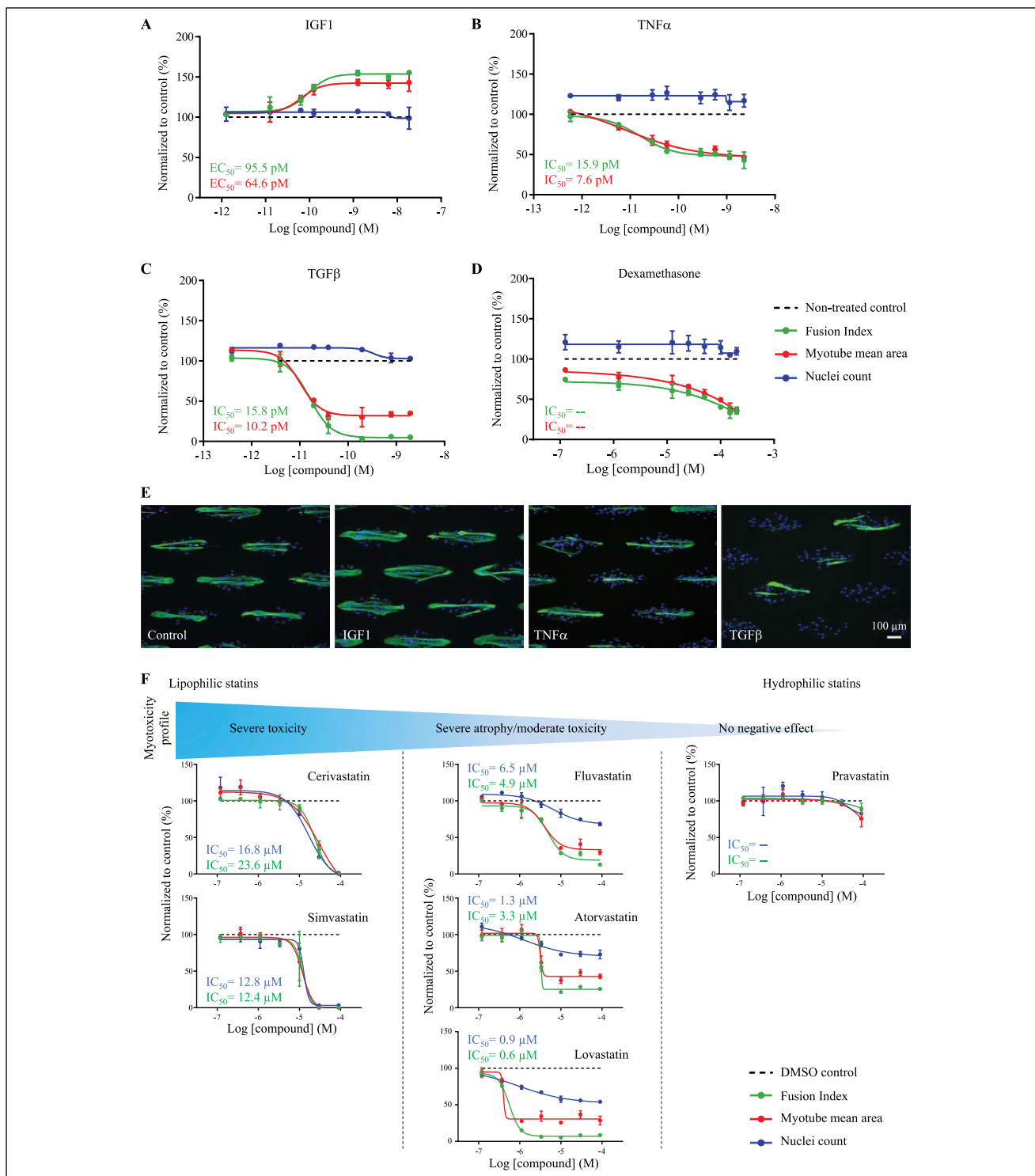


**Figure 3.** Pharmacological relevance of the MyoScreen platform for drug discovery. **(A–D)** Concentration–response curves showing the stimulatory and inhibitory effects of four hypertrophic or atrophic signaling compounds on fusion index (FI), myotube mean area, and nuclei count after 96 h of treatment. Data are normalized to vehicle control wells and show mean  $\pm$  SD;  $n$  = minimum of two wells. **(E)** Representative micrographs showing morphological changes in differentiated myotubes after treatment as described in this article, with different growth factors and cytokines provoking hypertrophy (2.5 nM insulin-like growth factor-I [IGF1]) or atrophy (0.57 nM tumor necrosis factor- $\alpha$  [ $TNF\alpha$ ] and 0.78 nM transforming growth factor- $\beta$  [ $TGF\beta$ ]). Images were automatically taken at 10 $\times$  magnification. Fluorescence double labeling using an anti-troponin T antibody (green) to indicate myotubes and Hoechst (blue) to stain nuclei. **(F)** Concentration–response curves comparing the effect of six statins on viability, FI, and myotube mean area and the correlation with statin lipophilicity. Myotubes were treated for 96 h as described in this article, and data are normalized to control wells;  $n$  = minimum of two wells. % activity and  $EC_{50}$  or  $IC_{50}$  values are summarized in **Supplementary Table S3**. (–):  $IC_{50}$  not calculable because response does not achieve a clear minimum even at the lowest concentration due to the limited range of applied concentrations. Primary myotube cultures from a 21-year-old male donor were used throughout this figure.

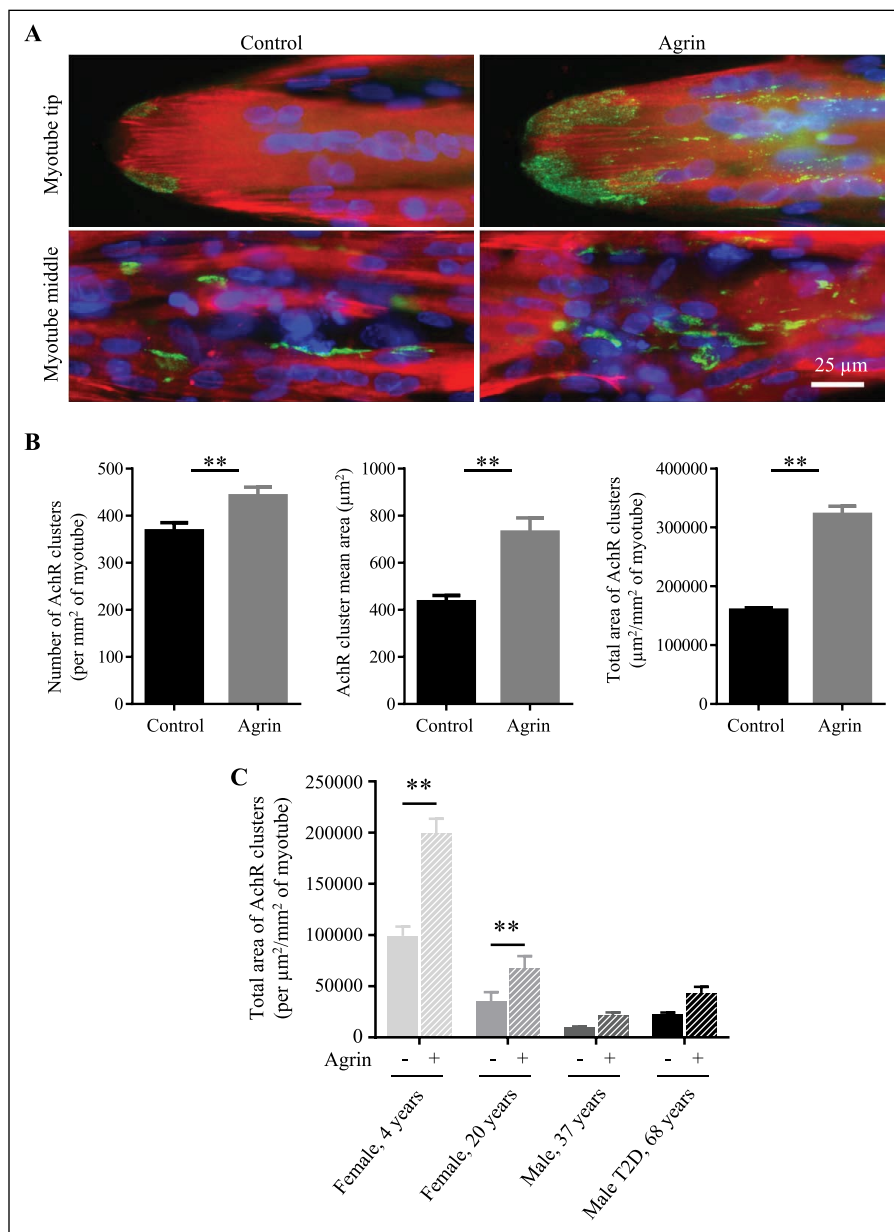


**Figure 4.** Modulation of acetylcholine receptor (AChR) aggregates by agrin. **(A)** Fluorescent images manually acquired with a wide-field microscope using a 20×/0.7 NA objective. Shown are AChR clusters (green) labeled with a specific anti-AChR antibody in troponin T–stained myotubes (red; female, 4 years) and nuclei stained with Hoechst (blue) under control and agrin-treated conditions. Note that AChR clusters preferentially concentrate in two different areas of parallel aligned myotubes, at the tips of myotubes and at the membrane of the central region of myotubes. **(B)** Automatized quantification of AChR aggregates shows that addition of 5 nM agrin for 16 h between days 7 and 8 of myotube differentiation in differentiation medium (DM) containing 2% horse serum (HS) induces an augmentation in the average size and total area of AChR clusters, compared with control myotubes. \*\**p* < 0.01 by Mann–Whitney statistical test (*n* = 6 wells). Primary myotube cultures from a 4-year-old female donor were used. **(C)** Characterization of postsynaptic membrane differentiation in myotubes cultured from 4 different donor samples. Myotubes were treated with 0.5 nM neural agrin between days 8 and 9 of differentiation for 16 h. Initial total AChR cluster area size correlates with donor age and increases after agrin treatment in all myotubes. *n* = 3 wells; \*\**p* < 0.01 based on Mann–Whitney test with comparison to control condition.

conditions (data not shown). The maturity of the postsynaptic membrane was explored in other donor cultures. All myotubes expressed spontaneous AChR clusters that doubled in size in response to agrin (Fig. 4C), indicating induction of postsynaptic NMJ differentiation. Initial AChR levels and cluster size decreased with donor age, however, in accordance with reports of NMJ fragmentation in aged muscle.<sup>2,5</sup>

### MyoScreen Myotubes Are Functional for ACh-Induced Postsynaptic Transmission and Contraction

In skeletal muscle *in vivo*, ACh activation of AChRs induces channel opening and local depolarization of the plasma

membrane, igniting an action potential that spreads along and into the myofiber, triggering release of stored calcium into the myoplasm and subsequent contraction. Autonomous contractions were occasionally visible in MyoScreen myotubes, indicating spontaneous discharge of action potentials (data not shown). To test the functionality of AChRs for postsynaptic signal transmission, transient changes in intracellular calcium concentration ( $[Ca^{2+}]_i$ ) were analyzed in response to stimulation by the neurotransmitter ACh, to mimic motor neuron input. To ensure maturation, calcium transients were measured by live cell fluorescent imaging of day 8–9 differentiated myotubes (male, 21 years) loaded with a calcium indicator, Fluo-4 AM. Addition of a bolus of 20 μM ACh induced a sharp (millisecond) fourfold increase

in Fluo-4 fluorescence, reflecting myotube excitation and an increase in myoplasmic  $\text{Ca}^{2+}$ . This was followed by a slower (seconds) decrease in Fluo-4 fluorescence to near-resting levels, which occurs during myotube contraction and relaxation, and resequestering of  $\text{Ca}^{2+}$  into the sarcoplasmic reticulum (SR; **Fig. 5A**). Changes in  $\text{Ca}^{2+}$  flux occurred in tandem with myotube contraction and relaxation observed during simultaneous phase-contrast videomicroscopy (**Suppl. Movie S1**). Similar  $\text{Ca}^{2+}$  kinetic data were obtained using Molecular Devices' FlexStation, which is designed for higher throughput measurements (data not shown). To verify the specificity of the ACh-triggered response, myotubes were preexposed to tubocurarine (100  $\mu\text{M}$ ), a competitive ACh inhibitor that binds to AChRs. Tubocurarine efficiently blocked ACh-elicited  $[\text{Ca}^{2+}]_i$  transients (**Fig. 5A**) and myotube contraction (data not shown), recapitulating *in vivo* properties of this muscle-relaxing agent. To mimic electrical stimulation, KCl at a submaximally activating concentration of 20 mM that depolarizes the plasma membrane was applied to myotubes (male, 19 years).  $[\text{Ca}^{2+}]_i$  increased by 2.2-fold (**Fig. 5B**) and activated contraction (**Suppl. Movie S2**). These results indicate the potential of MyoScreen myotubes for synaptic transmission in response to nervous excitation.

Relative changes in ACh-induced  $[\text{Ca}^{2+}]_i$  were compared in myotubes generated from biopsies from four individuals. Despite the low AChR expression in adult donors shown in **Figure 4C**, ACh still initiated  $[\text{Ca}^{2+}]_i$  increase, implying action potential propagation. Peak  $[\text{Ca}^{2+}]_i$  ranged from 3.2- to 5.4-fold but with no clear link to donor age, FI, or AChR levels (**Suppl. Fig. S4**).

### *MyoScreen Myotubes Have Attained ECC Comparable to That of Adult Skeletal Muscle*

ECC links excitation of the muscle fiber to contraction by electrochemical transduction and is regulated by high-voltage-activated dihydropyridine receptors (DHPRs) in the sarcolemma and ryanodine receptors (RyRs) in the SR membrane.<sup>3</sup> Evidence for the presence and activity of these two proteins was examined in day 8–9 differentiated MyoScreen myotubes using  $\text{Ca}^{2+}$  channel antagonists and agonists. Pre-exposure of myotubes (male, 21 years) to nifedipine (40  $\mu\text{M}$ ), a blocker of L-type  $\text{Ca}^{2+}$  channels including DHPRs, totally suppressed ACh-induced  $[\text{Ca}^{2+}]_i$  transients (**Fig. 5A**). Treatment of myotubes (male, 19 years), with 10 mM caffeine or 400  $\mu\text{M}$  4-CmC that opens RyR channels, provoked a 1.6- and 2.8-fold increase of  $[\text{Ca}^{2+}]_i$ , respectively (**Fig. 5B**), along with visible myotube contraction (**Suppl. Movie S3**). This pharmacological investigation establishes functional expression of the two main components of the ECC apparatus in MyoScreen myotubes.

During myogenesis, the ECC apparatus undergoes structural and functional maturation, acquiring a novel mechanism for controlling contraction. Immature skeletal muscle functions like cardiac muscle, with inflow of extracellular  $\text{Ca}^{2+}$  through DHPR channels essential for opening of RyR, calcium release, and contraction. In adult skeletal muscle, however, contraction is independent of extracellular  $\text{Ca}^{2+}$  and controlled via direct interaction of DHPR with RyR.<sup>35</sup> To ascertain the predominant mechanism operating in MyoScreen myotubes (female, 4 years),  $[\text{Ca}^{2+}]_i$  response to 20  $\mu\text{M}$  ACh was measured in the absence of extracellular  $\text{Ca}^{2+}$  ( $\text{Ca}^{2+}$ -free buffer supplemented with 2 mM EGTA). ACh still induced elevation of  $[\text{Ca}^{2+}]_i$ , indicating MyoScreen myotubes have acquired a mature ECC system (**Fig. 5C**). The increase in  $[\text{Ca}^{2+}]_i$  was smaller than that detected in 1.8 mM  $\text{Ca}^{2+}$  solution due to suppression of  $\text{Ca}^{2+}$  entry through AChRs and other channels in the plasma membrane that contribute >80% of total  $[\text{Ca}^{2+}]_i$  increase and prolong the  $\text{Ca}^{2+}$  transient (**Fig. 5C**).<sup>36</sup> Indeed, the decay phase of the transient in  $\text{Ca}^{2+}$ -free solution rapidly returned to basal levels, indicating  $\text{Ca}^{2+}$  removal mechanisms at work that are masked in the presence of extracellular  $\text{Ca}^{2+}$  influx. To verify that ACh action proceeds through RyRs, myotubes were pretreated with the RyR blocker, ryanodine (10  $\mu\text{M}$ ). Release of SR  $\text{Ca}^{2+}$  content was inhibited by comparable amounts in the absence and presence of extracellular  $\text{Ca}^{2+}$ , showing an equal proportion of mobilized  $\text{Ca}^{2+}$  originates from ryanodine-sensitive channels under both conditions (**Fig. 5C**). These data indicate that ECC occurs through DHPR physical interaction with RyRs and, by deduction, suggests the development of junctional triads that juxtapose the two proteins.<sup>3</sup> Indeed, extracellular calcium-independent ECC was detected in only the youngest myotube donor (female, 4 years), suggesting dependency on the degrees of differentiation and maturation reached by myotubes in culture (**Fig. 2B**).

### *MyoScreen Quantitative Contractile Activity Assay*

ACh (20  $\mu\text{M}$ ) stimulates myotubes to contract (**Suppl. Movie S1**), and at higher doses levels of contraction intensified, generating sufficient tension to pull myotubes off the cell-adhesive surface. This was observed as a retraction of one or both myotube extremities from the micropattern (**Fig. 5D**). The phenomenon was considered physiological, because pretreatment with AChR antagonist tubocurarine (100  $\mu\text{M}$ , 15 min) abrogated ACh-stimulated myotube detachment (**Fig. 5D**). To confirm that retraction is not due to death or damage of myotubes, an adenosine triphosphate (ATP)-based viability assay was performed after 5 min of incubation with ACh. ATP content was unchanged from that in control myotubes, even at ACh concentrations as high as

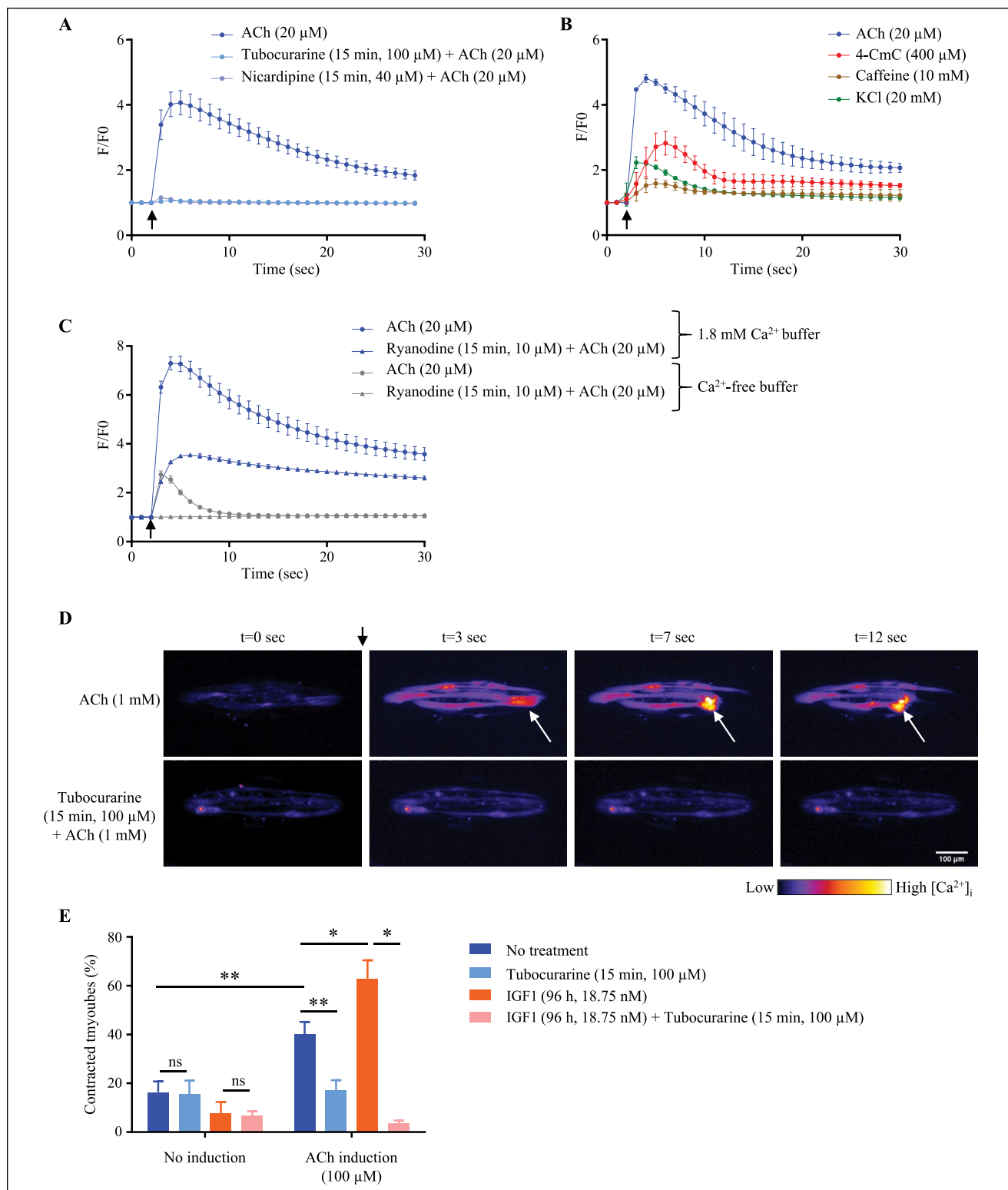


**Figure 5.** Excitation–contraction coupling (ECC) functionality and contraction response of MyoScreen myotubes treated with specific agonists or antagonists. **(A)** Cholinergic stimulation of day 9 differentiated MyoScreen myotubes (male, 21 years) with 20  $\mu\text{M}$  acetylcholine (ACh; dark blue line) causes an increase in  $[\text{Ca}^{2+}]_i$  as measured by  $\text{Ca}^{2+}$  imaging analysis.  $\text{Ca}^{2+}$  transients are completely inhibited by 15 min of pretreatment with 100  $\mu\text{M}$  tubocurarine (light blue line), a competitive antagonist of ACh, or 40  $\mu\text{M}$  nicardipine (gray line), a dihydropyridine receptor (DHPR) calcium-channel blocker. Arrow indicates onset of ACh application to the external buffer.  $n = 2$ –9 wells. **(B)** Representative traces of  $\text{Ca}^{2+}$  signals in day 8 differentiated myotubes (male, 19 years) after

(continued)

stimulation with 20  $\mu\text{M}$  ACh (dark blue line) or various other agonists. Arrow indicates when ACh or the agonist was added. The slower  $[\text{Ca}^{2+}]_i$  release dynamics compared to ACh and KCl are typical of the time delay needed for 4-CmC or caffeine to enter and reach their target in the myotube interior, as opposed to acting directly on the surface membrane.  $n = 2\text{--}3$  wells. (C) Temporal plot of  $[\text{Ca}^{2+}]_i$  induced by 20  $\mu\text{M}$  ACh in day 8 differentiated myotubes (female, 4 years) in the presence or absence of 1.8 mM extracellular calcium (circles). To resolve levels of  $\text{Ca}^{2+}$  release from intracellular stores, myotubes were pretreated with 10  $\mu\text{M}$  ryanodine in the two different buffers (triangles). Arrow indicates onset of ACh application to the external buffer.  $n = 2\text{--}4$  wells.

(D) Contraction and calcium release captured by time-lapse fluorescent microscopy imaging of day 5 differentiated myotubes (male, 21 years) before (0 s) and after stimulation (3 to 12 s) with 1 mM ACh (top panel). Myotubes pretreated with 100  $\mu\text{M}$  tubocurarine for 15 min before addition of 1 mM ACh (bottom panel). Black arrow indicates moment of ACh addition between 0 and 3 s. White arrows indicate a representative myotube retraction event resulting from contraction. Such events are never seen in the presence of the muscle-relaxing drug tubocurarine. Assignment of colors to  $[\text{Ca}^{2+}]_i$  is indicated by the horizontal color bar. (E) Quantification of contraction in myotubes (female, 20 years) that were differentiated during 5 days in the presence of vehicle or 18.75 nM IGF1 for 96 h, and subsequently treated or not with 100  $\mu\text{M}$  tubocurarine for 15 min before stimulation with 100  $\mu\text{M}$  ACh. Three minutes after contraction induction with ACh, myotubes were fixed, stained, and imaged, and the number of detached regions was automatically quantified. ns, statistically nonsignificant.  $n = 3\text{--}5$  wells; \* $p \leq 0.05$  and \*\* $p \leq 0.01$  calculated by Mann–Whitney analysis.

6 mM (Suppl. Fig. S5A). Accordingly, it was deduced that the number of retracted myotubes equates with the level of contraction and therefore contractile strength, also known as the degree of force or tension generated in muscle. Consequently, quantifying the number of retracted myotubes in fixed samples after ACh stimulation should allow indirect, yet rapid, assessment of contractile force.

To validate the potential of this approach for detecting compounds that affect myotube force-generating ability, IGF1, which is recognized to increase muscle size and strength in vitro and in vivo, was tested.<sup>14,37</sup> Myotubes (female, 20 years) at 5 days post differentiation were treated with 18.75 nM IGF1 for 96 h, and then stimulated to contract by adding 100  $\mu\text{M}$  ACh or vehicle control. Directly afterward, cells were fixed and processed for immunofluorescence and imaging. Automated quantification of the number of retracted myotubes showed that basal levels of contractile activity (i.e., passive tension)<sup>38</sup> in control and IGF1-treated myotubes in the absence of ACh stimulation were  $16.3 \pm 4.4\%$  and  $7.6 \pm 4.7\%$ , respectively (Fig. 5E, no induction). After ACh stimulation, myotubes treated with IGF1 showed a 1.57-fold increase in contractile activity compared to nontreated myotubes ( $40 \pm 5\%$  in control vs.  $63 \pm 8\%$  in IGF1-treated myotubes; Fig. 5E, ACh induction). The increase in number of contracted myotubes occurred only when stimulated by ACh, as exemplified in fluorescent images (Suppl. Fig. S5B). Furthermore, pretreatment with the relaxant drug tubocurarine (100  $\mu\text{M}$ ) before ACh stimulation reduced IGF1-enhanced ACh-stimulated contractile activity to baseline levels of passive tension measured in the absence of ACh (Fig. 5E). These experiments show that functional data concerning one aspect of muscle kinetics (i.e., myotube contractile force capacity) can be generated in a HT manner using the MyoScreen model.

### MyoScreen Phenotypic Screening for Molecules Promoting Muscle Regeneration

Despite inhibiting many systemic forms of muscle wasting in vivo, IGF1 is not a suitable therapeutic agent due to

adverse effects that include tumor growth and diabetes.<sup>37</sup> To find novel alternative compounds that promote healthy muscle regeneration and repair, a methodical screening strategy was undertaken, as schematized in **Supplementary Figure S6A**. MyoScreen myotubes (male, 21 years) were exposed to 2560 FDA-approved drugs or well-defined pharmacologically active compounds (10  $\mu\text{M}$  in monoplicate) combined from two chemical libraries (Prestwick and LOPAC<sup>1280</sup>). After 96 h of treatment, myotube differentiation, hypertrophy, and viability were quantified. Primary screening resulted in the identification of 29 hits (1.1% hit rate) that increased FI and/or myotube area to  $>^+40\%$  higher than the DMSO control mean, while maintaining viability between 78 and 120%, based on nuclei count (Fig. 6A and Suppl. Fig. 6B). Activity of 18.75 nM IGF1 was used as a positive control on each plate, and all 32 CYTOOplates passed quality control with a  $Z'$ -factor  $\geq 0.3$  (Suppl. Fig. 6C). Follow-up retesting in additional donors and at expanded doses confirmed 16/29 (55%) of compounds were dose-responsive (data not shown). These diverse chemicals grouped into five families based on molecular target, and they comprised novel and known pathways with links to muscle regeneration. One class is exemplified by tiratricol (FI: 169%; myotube area: 169.5%; Fig. 6A), a thyroid hormone analogue of which several members are recognized to stimulate skeletal muscle growth.<sup>39</sup> Subsequent hit expansion of the most active hits with the best potential suitability for therapeutic intervention resulted in the final retention of two drug candidates that belong to distinct chemical families and are described here as CYT3818 and CYT9733. Thus, at 10  $\mu\text{M}$ , CYT3818 significantly induced the FI in myoblasts from three out of four donors by  $+20\text{--}36\%$  according to the donor, and CYT9733 increased the FI in all donors by  $+11\text{--}72\%$ , comparable to the  $+18\text{--}65\%$  augmentation induced by IGF1 (Fig. 6B). CYT3818 and CYT9733 increased FI and myotube area in a dose-dependent manner with  $\text{EC}_{50}$  values of 7.5–11.4 pM and 1.6–2.6 nM, respectively, showing the higher potency of CYT3818 (Fig. 6C and Suppl. Fig. 6D). CYT9733, however, was

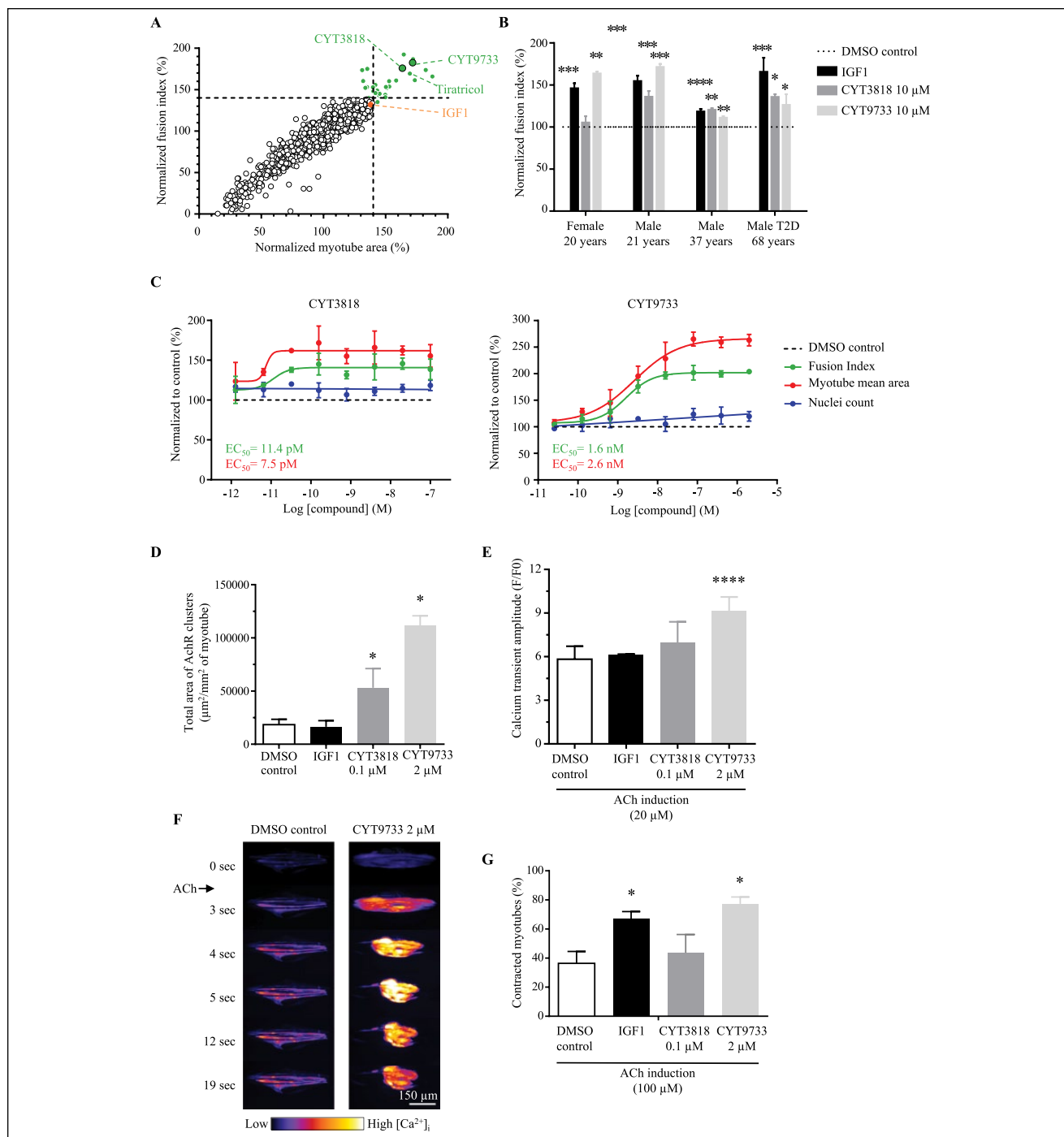


**Figure 6.** Primary screen results and hit characterization. **(A)** Fusion index (FI) and mean area effects for 2097 compounds out of the 2560 tested in total (10  $\mu$ M) normalized to DMSO control after 96 h of incubation on differentiating myotubes (male, 21 years). Exclusion criterion based on the nuclei count omitted compounds from further analysis that induced cytotoxicity at lower than 78% or increasing proliferation at higher than 120%. Compounds higher than the 140% cutoff threshold (dotted lines) are considered hits (green circles), 18.75 nM insulin-like growth factor-1 (IGF1) positive control is shown (orange circle), as well as tiratricol (small green circle) and two coded compounds selected for further analysis (large green circles). **(B)** Action of coded compounds on myotube differentiation in different donors. Myotubes were differentiated for 5 days with or without concomitant treatment for 4 days with 10  $\mu$ M of each compound or 0.01875  $\mu$ M IGF1. Cells were fixed and stained and quantified for FI (%) using high-content screening. Results are normalized to nontreated myotubes, shown as a dotted line at 100%. All compounds increase the FI higher than that of nontreated control myotubes, with different efficiencies according to the donor.  $n = 3$ –12 wells; \* $p \leq 0.05$ , \*\* $p \leq 0.01$ ,

(continued)

\*\*\* $p \leq 0.001$ , and \*\*\*\* $p \leq 0.0001$  as compared to control myotubes of each donor by Mann–Whitney test. **(C)** Eight-point dose–response curves for the two screen hits CYT3818 and CYT9733 using three phenotypic endpoints and myotubes cultured from a female, 20-year-old donor.  $EC_{50}$  values were calculated from fitted curves. **(D)** Effects of IGF1 and two lead compounds on AChR clusters in myotubes (female, 20 years) differentiated for 8 days in differentiation medium (DM) containing 2% horse serum (HS). Compounds were added 24 h after induction of differentiation.  $n = 3–6$  wells; \* $p \leq 0.05$  versus control myotubes by Mann–Whitney analysis. **(E)** Mean peak amplitudes of Fluo-4 fluorescence in 20  $\mu$ M ACh-stimulated myotubes (female, 20 years) differentiated for 8 days in DM containing 2% HS, of which 7 days were in the presence of IGF1, CYT3818, or CYT9733.  $n = 2–5$  wells; \*\*\*\* $p \leq 0.0001$  versus control myotubes by Mann–Whitney analysis. **(F)** Representative pseudo-color images extracted from a calcium flux experiment showing levels of intracellular free  $Ca^{2+}$  in myotubes (female, 20 years) before (0 s) and after stimulation with ACh (3 to 19 s). Myotubes were differentiated and treated or not with 2  $\mu$ M CYT9733 as described in this article. Note the strong increase in intracellular calcium concentration after ACh addition and the retraction of myotubes from the micropattern at 4 s in CYT9733-treated myotubes. Images were acquired every second in time-lapse mode using a Leica wide-field microscope at 10 $\times$  magnification. Assignment of colors to  $[Ca^{2+}]_i$  is indicated by the horizontal color bar. **(G)** Treatment of differentiating myotubes (female, 20 years) for 96 h with 2  $\mu$ M CYT9733 significantly increased the percentage of myotubes that exhibit strong contractions, detected as myotubes that retracted from the micropattern when stimulated with 100  $\mu$ M ACh. Number of contracted myotubes was comparable to that of IGF1-treated myotubes, while levels after CYT3818 treatment were not higher than those of controls.  $n = 4$  wells; \* $p \leq 0.05$  versus control myotubes by Mann–Whitney analysis.

more efficacious, with higher maximal response values for FI (203 vs. 141%) and inducing larger myotubes (265% vs. 166%). No toxic effects were observed for either compound as indicated by the cell count (**Fig. 6C** and **Suppl. Fig. 6D**). The positive influence of CYT3818 and CYT9733 on cell fusion rates suggests these compounds modify signaling pathways associated with myogenesis.

### MyoScreen Secondary Assays Provide Further Functional Readouts of Compound Activity

To further characterize the biological activities of CYT3818 and CYT9733, effects of the compounds were investigated on other aspects of myotube physiology, namely, AChR expression,  $Ca^{2+}$  flux, and contraction. All three assays were performed using the female, 20-year-old donor and 0.1  $\mu$ M CYT3818 or 2  $\mu$ M CYT9733, concentrations shown to induce maximum response in all donors (**Fig. 6B**), and the effects were compared to those of the reference compound, IGF1, at 18.75 nM. After 8 days of differentiation that included 7 days of drug treatment, myotubes treated with CYT3818 and CYT9733 showed substantially more AChR clusters (data not shown), and total AChR area increased by three- and sixfold, respectively, while IGF1 had no effect (**Fig. 6D**). In the case of  $Ca^{2+}$  flux measurements after ACh stimulation, only myotubes differentiated in the presence of CYT9733 showed a statistically significant increase of 1.56-fold in  $[Ca^{2+}]_i$  peak amplitude compared to control myotubes (**Fig. 6E**). Again, IGF1 had no effect. Calcium flux time-lapse videos also implied that myotubes differentiated in the presence of CYT9733 displayed a marked increase in the number of retracting myotubes after ACh stimulation (**Fig. 6F**). The effect on contraction force was therefore quantified after 5 days of differentiation that included 4 days of CYT3818, CYT9733, or IGF1 treatment. When stimulated by addition of 100  $\mu$ M

ACh, active contractile force augmented in all experimental conditions, but especially in myotubes treated with CYT9733 (77  $\pm$  5%) and IGF1 (67  $\pm$  5%). Meanwhile, CYT3818 resulted in contractile activity (44  $\pm$  13%) that was slightly higher than that of control myotubes (36  $\pm$  8%), suggesting that CYT3818 has some ability, if not a significant one, to induce contraction (**Fig. 6G**).

Collectively, the MyoScreen functional assays discriminate between the properties of the two candidate compounds and indicate a difference in their MOA compared to IGF1. Both CYT3818 and CYT9733 increase myogenic differentiation, induce hypertrophy, and, contrary to IGF1, augment AChR cluster count and size. CYT9733 demonstrates additional activities, enhancing ACh-stimulated  $[Ca^{2+}]_i$  influx and contraction force, perhaps suggesting a mechanism whereby CYT9733 supplies more available  $Ca^{2+}$  to contractile proteins, potentiating stronger contraction. Overall, these results validate MyoScreen as a complete in vitro screening platform, amenable to large-scale screening as well as compound characterization.

### Discussion

Under conventional cell-culture conditions, non-innervated primary human skeletal muscle cells do not accumulate AChR clusters or spontaneously contract.<sup>34</sup> A major block, therefore, for phenotypic screening in muscle drug discovery has been a lack of suitable human-derived models. By exploiting micropatterns, MyoScreen overcomes the biological limitations of conventional cultures and the technical disadvantages of 3D muscle bundles, providing contracting myotubes that possess functional AChRs necessary for NMJ formation and a baseline for screening in a skeletal muscle model that is closer to that of mature myofibers. As well as providing enhanced myogenesis when differentiated in CYTOOplates, the MyoScreen myotubes

are functionally more mature compared to conventionally cultured myotubes, as evidenced by

- 1) Higher levels of myofibrillogenesis with extensive cross-striations
- 2) AChRs clusters that form independently of agrin and innervation
- 3) Extracellular  $\text{Ca}^{2+}$ -independent ECC typical of mature skeletal muscle
- 4) Transient  $[\text{Ca}^{2+}]_i$  increase and contraction in response to ACh, KCl, and caffeine

These advanced maturation characteristics are likely physiologically dependent on uniaxial length–tension that can develop throughout organized anisotropic myotubes aligned transversely in CYTOOplates. In contrast, in isotropic myotubes growing haphazardly in conventional cell culture, such tension forces are multiaxial and transient, being subject to shape changes and a probable reason for the lack of relevant features in these cells. The new screenable phenotypes intrinsic to MyoScreen myotubes create an opportunity to develop HT assays that normally needed 3D muscle myobundles to express AChRs and analyze active contraction.<sup>14,20</sup> Furthermore, with standardized dimensions and orientation, MyoScreen myotubes resolve many image analysis hurdles and provide the robustness and reproducibility required for quantitative analysis of morphological parameters and detection of small changes induced by pharmaceutical and cell-based therapeutics.

Results from four donors show that MyoScreen can differentiate inherent phenotypic properties related to ageing, allowing an appropriate starting point for comparative analyses and personalized platforms. Furthermore, based on the accurate response to commonly prescribed pharmaceuticals known to cause adverse effects of muscle weakness and wasting, such as corticosteroids exemplified by dexamethasone and statins such as simvastatin (Fig. 3D and 3F), the MyoScreen model and assays are expected to be predictive and clinically relevant. Future approaches will extend to disease modeling of genetic musculoskeletal and neuromuscular disorders using patient-derived myoblasts and human pluripotent stem cells. Nerve–muscle co-culture will further render MyoScreen suitable for screening compounds that improve AChR formation and maturation for the treatment of neuromuscular dysfunction or that rescue pathological alterations of NMJs, as occurs in age-related muscle wasting.

The MyoScreen platform holds vast potential for applications linked to nutraceuticals, livestock meat production, and toxicology, and it has generated standardized myotubes from primary porcine, L6 rat, and C2C12 mouse cell lines with the detection of morphological hypertrophy or atrophy response to appropriate inducers (data not shown). Other recent developments include transfer of the MyoScreen assays to the

384-well CYTOOplate format, with no significant alteration in assay range or sensitivity. Furthermore, MyoScreen myotubes are amenable to transfection by small interfering RNAs, enabling genome-scale functional screening, and are efficiently infected by recombinant adeno-associated viruses, providing in vitro testing of new therapeutic proteins for gene therapy of muscle diseases (data not shown).

With the objective of ameliorating muscle regeneration and repair after atrophy or injury, two compounds with pharmacological potential as new myogenic inducers were identified in a screen using myoblasts undergoing differentiation. Further investigation using functional assays established in this report determined that both candidates induce AChR clustering and contraction, particularly in the case of CYT9733 (Fig. 6D and 4G). Because myofiber size is a poor indicator of muscle strength,<sup>40</sup> the contractile activity assay is extremely useful for rapidly selecting hypertrophy-inducing compounds associated with an improved capacity to produce force, such as IGF1.<sup>14,37</sup> Despite IGF1 being a well-studied hypertrophiant that increases protein synthesis and contraction, the intracellular mechanisms responsible for the latter activity remain obscure and presumably different from those of CYT9733, which in addition positively influenced  $[\text{Ca}^{2+}]_i$  levels (Fig. 6E).

Preclinical animal studies are now needed to evaluate CYT3818 and CYT9733 as potential therapeutics to repair damaged skeletal muscle or increase muscle mass and strength, and hence improve muscle wasting and weakness associated with aging, cachexia, diabetes, myotoxic injury, and inherited myopathies.

### Acknowledgments

We thank Dr. Michel Bornens and colleagues for useful discussions and plate production.

### Declaration of Conflicting Interests

The authors declared the following potential conflicts of interest with respect to the research, authorship, and/or publication of this article: Some authors are employees of CYTOO SA, a preclinical-stage biotechnology company that uses MyoScreen as a drug discovery engine for neuromuscular diseases.

### Funding

The authors disclosed receipt of the following financial support for the research, authorship, and/or publication of this article: Work was financed by Bpifrance as part of France's Industrial Strategic Innovation (ISI) grant program with the project title "Evolved Tissue Inspired Cell Systems" (ETICS; contract no. 1107018W).

### References

1. Bursac, N.; Juhas, M.; Rando, T. A. Synergizing Engineering and Biology to Treat and Model Skeletal Muscle Injury and Disease. *Ann. Rev. Biomed. Eng.* **2015**, *17*, 217–242.

2. Bloch-Gallego, E. Mechanisms Controlling Neuromuscular Junction Stability. *Cell Mol. Life Sci.* **2015**, *72* (6), 1029–1043.
3. Rebbeck, R. T.; Karunasekara, Y.; Board, P. G.; et al. Skeletal Muscle Excitation-Contraction Coupling: Who Are the Dancing Partners? *Int. J. Biochem. Cell Biol.* **2014**, *48*, 28–38.
4. Cohen, S.; Nathan, J. A.; Goldberg, A. L. Muscle Wasting in Disease: Molecular Mechanisms and Promising Therapies. *Nat. Rev. Drug Discov.* **2015**, *14* (1), 58–74.
5. Tintignac, L. A.; Brenner, H. R.; Ruegg, M. A. Mechanisms Regulating Neuromuscular Junction Development and Function and Causes of Muscle Wasting. *Physiol. Rev.* **2015**, *95* (3), 809–852.
6. Gintjee, T. J.; Magh, A. S.; Bertoni, C. High Throughput Screening in Duchenne Muscular Dystrophy: From Drug Discovery to Functional Genomics. *Biology (Basel)* **2014**, *3* (4), 752–780.
7. Engler, A. J.; Griffin, M. A.; Sen, S.; et al. Myotubes Differentiate Optimally on Substrates with Tissue-Like Stiffness: Pathological Implications for Soft or Stiff Microenvironments. *J. Cell Biol.* **2004**, *166* (6), 877–887.
8. Cooper, S. T.; Maxwell, A. L.; Kizana, E.; et al. C2C12 Co-Culture on a Fibroblast Substratum Enables Sustained Survival of Contractile, Highly Differentiated Myotubes with Peripheral Nuclei and Adult Fast Myosin Expression. *Cell Motil. Cytoskeleton* **2004**, *58* (3), 200–211.
9. Yamamoto, D. L.; Csikasz, R. I.; Li, Y.; et al. Myotube Formation on Micro-Patterned Glass: Intracellular Organization and Protein Distribution in C2C12 Skeletal Muscle Cells. *J. Histochem. Cytochem.* **2008**, *56* (10), 881–892.
10. Rakhilin, S.; Turner, G.; Katz, M.; et al. Electrical Impedance as a Novel Biomarker of Myotube Atrophy and Hypertrophy. *J. Biomol. Screen.* **2011**, *16* (6), 565–574.
11. Agle, C. C.; Velloso, C. P.; Lazarus, N. R.; et al. An Image Analysis Method for the Precise Selection and Quantitation of Fluorescently Labeled Cellular Constituents: Application to the Measurement of Human Muscle Cells in Culture. *J. Histochem. Cytochem.* **2012**, *60* (6), 428–438.
12. Ostrovidov, S.; Hosseini, V.; Ahadian, S.; et al. Skeletal Muscle Tissue Engineering: Methods to Form Skeletal Myotubes and Their Applications. *Tissue Eng. Part B Rev.* **2014**, *20* (5), 403–436.
13. Sebastian, S.; Goulding, L.; Kuchipudi, S. V.; et al. Extended 2D Myotube Culture Recapitulates Postnatal Fibre Type Plasticity. *BMC Cell Biol.* **2015**, *16*, 23.
14. Vandenburg, H.; Shansky, J.; Benesch-Lee, F.; et al. Drug-Screening Platform Based on the Contractility of Tissue-Engineered Muscle. *Muscle Nerve* **2008**, *37* (4), 438–447.
15. Wang, L.; Shansky, J.; Vandenburg, H. Induced Formation and Maturation of Acetylcholine Receptor Clusters in a Defined 3D Bio-Artificial Muscle. *Mol. Neurobiol.* **2013**, *48* (3), 397–403.
16. Das, M.; Rumsey, J. W.; Bhargava, N.; et al. Skeletal Muscle Tissue Engineering: A Maturation Model Promoting Long-Term Survival of Myotubes, Structural Development of the Excitation-Contraction Coupling Apparatus and Neonatal Myosin Heavy Chain Expression. *Biomaterials* **2009**, *30* (29), 5392–5402.
17. Guo, X.; Greene, K.; Akanda, N.; et al. In Vitro Differentiation of Functional Human Skeletal Myotubes in a Defined System. *Biomater. Sci.* **2014**, *2* (1), 131–138.
18. Yamamoto, Y.; Ito, A.; Fujita, H.; et al. Functional Evaluation of Artificial Skeletal Muscle Tissue Constructs Fabricated by a Magnetic Force-Based Tissue Engineering Technique. *Tissue Eng. Part A* **2011**, *17* (1–2), 107–114.
19. Ikeda, K.; Ito, A.; Imada, R.; et al. In Vitro Drug Testing Based on Contractile Activity of C2C12 Cells in an Epigenetic Drug Model. *Sci. Rep.* **2017**, *7*, 44570.
20. Madden, L.; Juhas, M.; Kraus, W. E.; et al. Bioengineered Human Myobundles Mimic Clinical Responses of Skeletal Muscle to Drugs. *Elife* **2015**, *4*, e04885.
21. Cash, J. N.; Angerman, E. B.; Kirby, R. J.; et al. Development of a Small-Molecule Screening Method for Inhibitors of Cellular Response to Myostatin and Activin A. *J. Biomol. Screen.* **2013**, *18* (7), 837–844.
22. Cross-Doersen, D.; Isfort, R. J. A Novel Cell-Based System for Evaluating Skeletal Muscle Cell Hypertrophy-Inducing Agents. *In Vitro Cell Dev. Biol. Anim.* **2003**, *39* (10), 407–412.
23. Courdier-Fruh, I.; Barman, L.; Briguet, A.; et al. Glucocorticoid-Mediated Regulation of Utrophin Levels in Human Muscle Fibers. *Neuromuscul. Disord.* **2002**, *12* (Suppl. 1), S95–S104.
24. Baudy, A. R.; Saxena, N.; Gordish, H.; et al. A Robust in Vitro Screening Assay to Identify NF-KappaB Inhibitors for Inflammatory Muscle Diseases. *Intl. Immunopharmacol.* **2009**, *9* (10), 1209–1214.
25. Vandenburg, H.; Shansky, J.; Benesch-Lee, F.; et al. Automated Drug Screening with Contractile Muscle Tissue Engineered from Dystrophic Myoblasts. *FASEB J.* **2009**, *23* (10), 3325–3334.
26. Schindelin, J.; Rueden, C. T.; Hiner, M. C.; et al. The ImageJ Ecosystem: An Open Platform for Biomedical Image Analysis. *Mol. Reprod. Dev.* **2015**, *82* (7–8), 518–529.
27. Huang, N. F.; Lee, R. J.; Li, S. Engineering of Aligned Skeletal Muscle by Micropatterning. *Am. J. Transl. Res.* **2010**, *2* (1), 43–55.
28. Junkin, M.; Leung, S. L.; Whitman, S.; et al. Cellular Self-Organization by Autocatalytic Alignment Feedback. *J. Cell Sci.* **2011**, *124* (Pt 24), 4213–4220.
29. Bajaj, P.; Reddy, B., Jr.; Millet, L.; et al. Patterning the Differentiation of C2C12 Skeletal Myoblasts. *Integr. Biol. (Camb.)* **2011**, *3* (9), 897–909.
30. Pietrangolo, T.; Puglielli, C.; Mancinelli, R.; et al. Molecular Basis of the Myogenic Profile of Aged Human Skeletal Muscle Satellite Cells during Differentiation. *Exp. Gerontol.* **2009**, *44* (8), 523–531.
31. Pereira, R. M.; Freire de Carvalho, J. Glucocorticoid-Induced Myopathy. *Joint Bone Spine* **2011**, *78* (1), 41–44.
32. Zipes, D. P.; Zvaifler, N. J.; Glasscock, R. J.; et al. Rosuvastatin: An Independent Analysis of Risks and Benefits. *MedGenMed* **2006**, *8* (2), 73.
33. Zhang, J. H.; Chung, T. D.; Oldenburg, K. R. A Simple Statistical Parameter for Use in Evaluation and Validation of

- High Throughput Screening Assays. *J. Biomol. Screen.* **1999**, *4* (2), 67–73.
34. Gajsek, N.; Jevsek, M.; Mars, T.; et al. Synaptogenetic Mechanisms Controlling Postsynaptic Differentiation of the Neuromuscular Junction Are Nerve-Dependent in Human and Nerve-Independent in Mouse C2C12 Muscle Cultures. *Chem. Biol. Interact.* **2008**, *175* (1–3), 50–57.
35. Calderon, J. C.; Bolanos, P.; Caputo, C. The Excitation-Contraction Coupling Mechanism in Skeletal Muscle. *Biophys. Rev.* **2014**, *6* (1), 133–160.
36. Grassi, F.; Fucile, S.; Eusebi, F. Ca<sup>2+</sup> Signalling Pathways Activated by Acetylcholine in Mouse C2C12 Myotubes. *Pflugers Arch.* **1994**, *428* (3–4), 340–345.
37. Philippou, A.; Barton, E. R. Optimizing IGF-I for Skeletal Muscle Therapeutics. *Growth Horm. IGF Res.* **2014**, *24* (5), 157–163.
38. Magid, A.; Law, D. J. Myofibrils Bear Most of the Resting Tension in Frog Skeletal Muscle. *Science* **1985**, *230* (4731), 1280–1282.
39. Salvatore, D.; Simonides, W. S.; Dentice, M.; et al. Thyroid Hormones and Skeletal Muscle: New Insights and Potential Implications. *Nat. Rev. Endocrinol.* **2014**, *10* (4), 206–214.
40. Hoffman, E. P.; Escolar, D. Translating Mighty Mice into Neuromuscular Therapeutics: Is Bigger Muscle Better? *Am. J. Pathol.* **2006**, *168* (6), 1775–1778.